Application of DIC technique to concrete – study on objectivity of measured surface displacements

Ł. Skarżyński, J. Kozicki and J. Tejchman

Faculty of Civil and Environmental Engineering

Gdańsk University of Technology, Poland

lskarzyn@pg.gda.pl, jkozicki@pg.gda.pl, tejchmk@pg.gda.pl

Abstract

The measurements of the width of a localized zone on the surface of notched concrete beams under quasi-static three-point bending were performed using the 2D Digital Image Correlation technique. Different image length resolutions, image search patches and distances between search patch centres were tested. Attention was paid to the accuracy and objectivity of surface displacements measured. An original method was proposed to determine the width of localized zones based on experiments.

Keywords: concrete beam, Digital Image Correlation, localized zone width, surface displacement, three-point bending

---

1. Introduction

Fracture process is a fundamental phenomenon in concrete materials [1]-[3]. During a fracture process, micro-cracks first arise before the peak on the stress-strain curve which change gradually during material softening into dominant distinct macroscopic cracks up to rupture. Thus, a fracture process is generally subdivided into 2 main stages: appearance of narrow regions of intense deformation (equivalent to the region of intense micro-cracking) ahead of macro-cracks and occurrence of discrete macro-cracks.

A realistic description of localized zones (called also fracture process zones FPZs) in concrete (their width, length, shape and distance), which are not negligibly small as compared to the specimen size [1], is of a major importance to understand degradation problems in concrete, ensure safety and durability of concrete and reinforced concrete structures, to predict and optimize the concrete

behaviour and to determine a combined deterministic-statistical size effect. It is also extremely important to determine a characteristic length of micro-structure in continuum crack models for cementitious materials and a transition phase in coupled continuous-discontinuous crack approaches [3]. This length is introduced into continuum models via e.g. non-local or strain-gradient theories to properly describe the size of localized zones, to obtain mesh-independent finite element results and to capture a deterministic size effect [1], [3-5].

A direct observation of a fracture process is difficult because of a small scale at which micro-structural events interact with a failure process. Different techniques have been used to experimentally investigate a fracture process in quasi-brittle materials (concrete, rock and masonry) at the laboratory scale such as: digital image correlation (DIC) [6-11], electron microscope scanning [12-15], acoustic emission [16-18] and X-rays [19]. Recently, the most popular method (due to its availability, simplicity and low cost) has become the DIC technique, wherein material displacements are obtained by tracking the deformation of a random speckle pattern applied to the surface through digital images acquired at different instances of deformation. Next strains, which are the best indicator for localized zones, based on displacements are calculated using standard finite-element shape functions. The method gives high resolution measurements of a displacement field [20]. It can be used both for 2D and 3D measurements [21]. For concrete, strain localization and crack size can be both easily identified [10], useful since they are two key parameters needed to estimate the permeability, strength and durability of structural concrete components [1].

The intention of our research works was to measure in two dimensions the size and shape of a localized zone on the surface of notched fine-grained concrete beams under three-point bending by means of the DIC technique in order to determine a characteristic length of micro-structure in continuum concrete models based on comparative FE analyses [3], [23]. Special attention was paid to the objectivity of measured displacements on the beams' surface during the development of a localized zone as a function of the length resolution (in pixels per mm), the search patch size of images and the distance between search patch centres. To process digital images and to determine the strain localization size, our software [8], [9] was applied. For verification purposes, the commercial software VIC-2D [22] was also used. The presented research work is the extension of our earlier investigations of strain localization in notched concrete beams using DIC [9], [23]. In this paper, an original method was proposed for determining precisely and uniformly the width of a localized zone in concrete based on experimental results.

2. Digital Image Correlation technique

DIC is an optical and non-contact measurement method to visualize surface displacements by successive post-processing of digital images taken with a constant time between frames from a professional digital camera [24-26]. The coloured surface serves as a tracer in concrete. The digital camera sensors are comprised of tiny, light-sensitive elements called pixels. When an image is captured, each pixel reflects three numbers (called the colour components YC_bC_r) in proportion to the amount of the light reflected from the imaged object, where Y is the luminosity (brightness), C_b is the blueness and C_r is the redness. The DIC system interprets differences in light intensity as a gray-scale pattern recorded at each pixel on CCD-camera (Charge Coupled Device). Three functions are of a major importance for DIC: a) image field intensity, b) cross-correlation function and c) interpolation function. The image intensity field assigns to each point in the image plane a scalar value which reflects the light intensity (Y-colour component) of the corresponding point in the physical space (it maps simply the light energy of an individual particle in a physical space). The gray levels range numerically between 0 (black) and 255 (white) for an 8-bit image. A so-called area of interest is cut out of the digital image and small overlapping sub-areas called search sub-sets (patches or windows) are chosen. If the deformation between two images is sufficiently small, the patterns of the interrogation cells are supposed not to change their characteristics (only their locations). A displacement pattern is detected by comparing two consecutive images captured by a camera which remains in a fixed position with its axis oriented perpendicularly to the plane of deformation. To find a local displacement between images '1' and '2', a search zone is extracted from the second image. A correct local displacement vector for each interrogation cell is accomplished by means of a cross-correlation function between two consecutive brightness distributions in two digital images. The function calculates simply possible displacements by correlating all gray values from the first image with all gray values from the second image. The correlation plane is evaluated at single pixel intervals, what means that the resolution is equal to one pixel. By fitting an interpolation function to the region close to the peak, the displacement vector is established with a high accuracy (equal to the correlation offset). The peak in the correlation function indicates that two images are overlaying each other (thus, it indicates the 'degree of match' between two images).

In our own method we used the Pearson's product-moment correlation function [8], [9] during the evaluation of experimental outcomes. The peak (equivalent to the best match) of the correlation function is usually not clearly distinguished as the correlation function produces results for each

3

pixel of image. To precisely locate the peak, a sub-pixel interpolation was performed. As an interpolation function, the function sinc256 was used. It has been shown that the accuracy in strain measurements when compared with strain gauge data is within $\pm200\mu$ [27]. A general procedure to evaluate DIC displacement measurements errors was proposed by Bornert et al. [20]. The accuracy of DIC depends obviously strongly on the strain magnitude in the material tested.

The DIC technique has been several times used for concrete. In the experiments by Alam et al. [11], and Robert et al. [28] and Ferreira et al. [29] (concrete under bending), by Choi and Shah [30] (concrete under compression) and by Corr et al. [31] (concrete during pulling), strain localization was not investigated. In turn, Wu et al. [32] investigated a localized zone in concrete beams under three point bending with the maximum aggregate size of 8 mm. The width of a localized zone estimated on the basis of strain contours was 2.8 mm ($0.35 \times d_{max}$), where d_{max} – the maximum aggregate size) at the peak load. The maximum localized zone height was about 25.5 - 44 mm [$(0.55-0.65) \times D$], where D – the beam height).

Alternatively, some researchers used the 3D acoustic emission technique to investigate micro-cracking properties of concrete [6], [33], [34]. The width of a micro-crack region was about 70 mm ($2.8 \times d_{max}$) [33], 40 mm ($2.9 \times d_{max}$) [34]. In turn, the height of a micro-crack region was about 75 mm ($0.125 \times D$) [33], 80 mm ($0.55 \times D$) [34], 54.9 mm ($0.77 \times D$) [3]. When using X-rays [19], [35], the width of a localized zone was 6.5 mm ($5.4 \times d_{max}$) [16] and 20-45 mm [$(2.25-4) \times d_{max}$] [35], and the height was 16 mm ($0.4 \times D$) [19] and 30-40 mm (($0.375-0.5) \times D$), respectively [35]. In turn, the measured width of a localized zone was 33 mm ($2.35 \times d_{max}$) and the height 90 mm ($0.4 \times D$) [15] during application of a scanning electron microscope technique.

Summarized, strain localization in concrete significantly depends on the material micro-structure, specimen size and deformation type. The width of a localized zone is also affected by the measurement technique applied due to the low magnitude of deformation.

3. Experiments with concrete beams

The experimental program and studies on the objectivity of experimental results by DIC included three-point bending laboratory tests carried out on fine-grained concrete beams with free ends (height D=80 mm, length L=320 mm, span s=$3D$=240 mm and thickness b=40 mm) (Figs.1 and 2) under quasi-static conditions [9], [23]. A notch of the height of $D/10$=8 mm and width of 3 mm was

4

located at the mid-span. The tests were performed with a controlled notch opening displacement velocity (or crack mouth opening displacement CMOD rate) of 0.002 mm/min. This type of control allowed obtaining a gradual displacement increase and a steady strength decrease in a post-peak regime. A CMOD gauge was located below the beam notch.
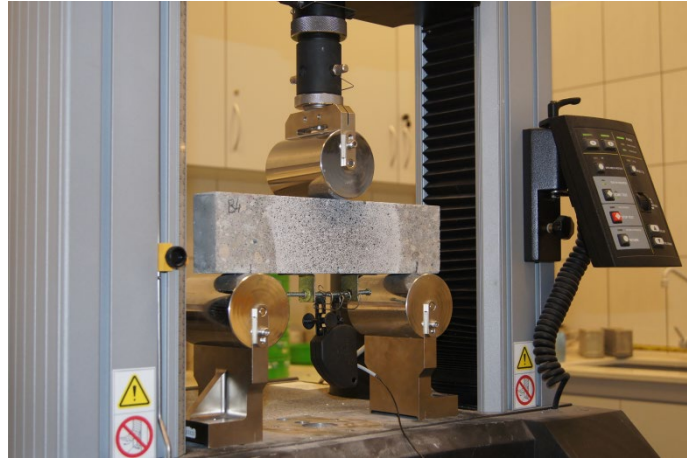

Fig.1: Concrete small-size beam in servo testing machine
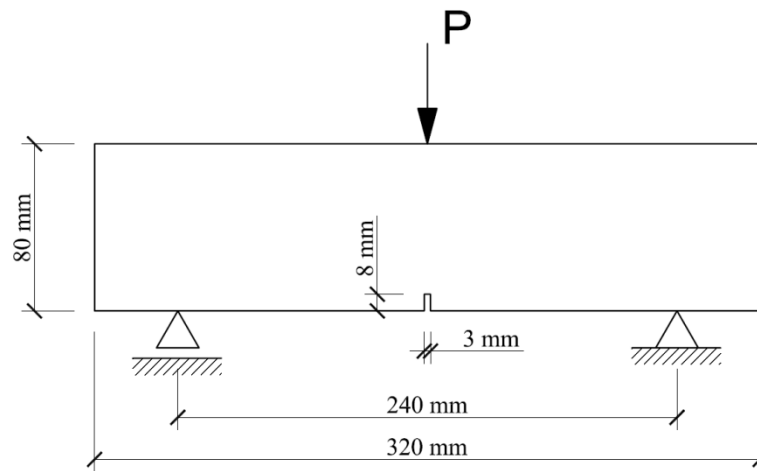

Fig.2: Geometry of experimental concrete small-size beam subjected to three-point bending (*P* – vertical force) [9]

A fine-grained concrete mix was composed of the ordinary Portland cement (CEM I 32.5 R), water and sand (with the mean aggregate diameter $d_{50} \approx 0.5$ mm and d_{max}=2.0 mm). The water to cement ratio *w/c* was equal 0.5. The beams were cut out from the same mix block. The uniaxial compression strength determined after 28 days on cubes of $10 \times 10 \times 10$ cm^3 was f_c=51.2 MPa.

5

In the experiments, the digital camera Canon EOS-1Ds Mark II with the powerful 16.7 megapixels CMOS sensor was applied. It was mounted on a tripod with its axis perpendicular to the photographed specimen surface. The concrete beams were initially carefully polished and painted white. Next, a speckle pattern (serving as a tracer) was put on this surface using a black colour spray. The digital photos were shot every 6 s. The camera was fixed at the certain distance from the beam in order to provide the images with the area of 35×20 mm2 (case '1' - beams 'A1', 'A2' and 'A3') or with the area of 95□60 mm2 (case '2' - beams 'B1' and 'B2') above the beam notch (using always the same image resolution of 3546 pixels × 2304 pixels). Thus, one pixel in the case '1' represented approximately the square of 10 μm (the length resolution was about 90 pixel/mm) and in the case '2' the square of 27 μm (the length resolution was about 30 pixel/mm) on the beam surface.

4. Test results with concrete beams

Five arbitrary experimental curves from 5 different tests of the vertical force P on the beam top versus the horizontal CMOD under the notch with a fine-grained concrete beam of Fig.1 are presented in Fig.3. The measured curves were different before and after the peak load due to a strongly heterogeneous internal structure of concrete. The maximum measured vertical force was P_{max}=1.45-1.70 kN at CMOD equal to 0.02-0.04 mm. The tensile strength was about 2.6 MPa and deflection at P_{max} was u=0.3 mm (u/D=0.00375). The softening rate was similar in all tests.

A localized zone with a different shape forms always on the concrete beam surface of Fig.2 above the notch. A localized zone is always strongly curved [9] and may even create branches (Fig.4). It can be well recognized at the peak load based on the horizontal displacement and horizontal normal strain profiles across a localized zone above the notch (Fig.4).

In order to determine the width of a localized zone (Fig.4a), the measured surface displacements from DIC (Fig.4b) were fitted by the error function ERF (Eq.1, Fig.5a), being a special function of a sigmoid shape, whereas the surface strains calculated from the displacements (Fig.4c) were fitted by the usual normal distribution (Gauss) function (Eq.2, Fig.5b):

$$ERF(x) = \frac{2}{\pi} \int_0^x e^{-t^2} dt \qquad (1)$$

and

$$f\left(\mathrm{x},\sigma\right)=\frac{1}{\sigma\sqrt{2\pi}}e^{-\frac{1}{2}\left(\frac{x}{\sigma}\right)^2} \tag{2}$$

The halved error function evaluated at $\dfrac{x}{\sigma\sqrt{2}}$ for positive x values gives the probability that a measurement under the influence of normally distributed errors with the standard deviation σ has a distance less than x from the mean value.
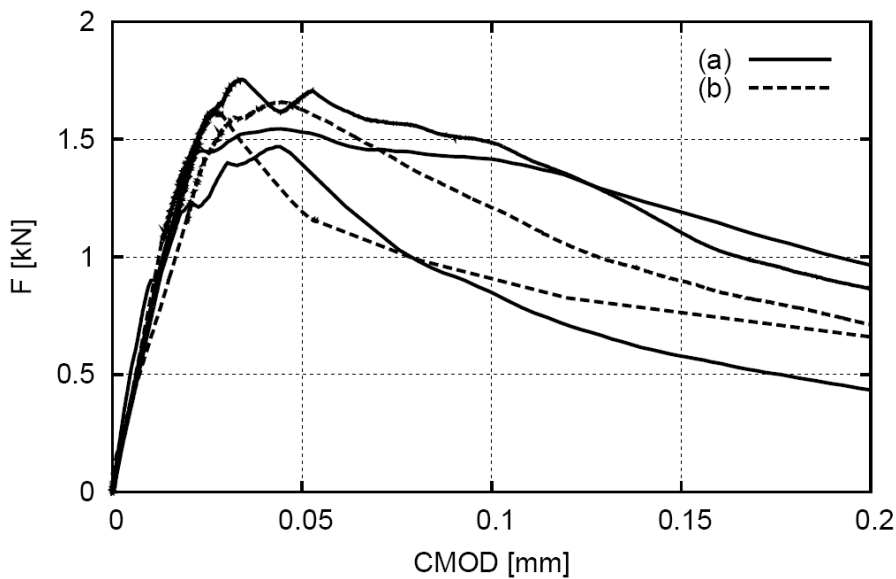

Fig.3: Five experimental vertical forces - horizontal CMOD curves for fine-grained concrete beam: a) image size was 35×20 mm^2 (image length resolution 90 pixel/mm), b) image size was 95×60 mm^2 (image length resolution 30 pixel/mm)

4.1 Effect of image parameters
Effect of search patch size

The effect of the search patch size on the width of a localized zone based on the horizontal displacement and horizontal normal strain above the beam notch at peak load is shown in Figs.6 and 7, using the high length resolution of 90 pixels/mm and the distance of search patch centres of 15 pixels. This effect is also shown at two different length resolutions in Tabs.1 and 2, when the measured surface displacements were fitted by the error function (Eq.1) and the surface strains were fitted by the normal distribution (Gauss) function (Eq.2). In all cases, our own software [8], [9] and a commercial software VIC-2D [22] were used in parallel.
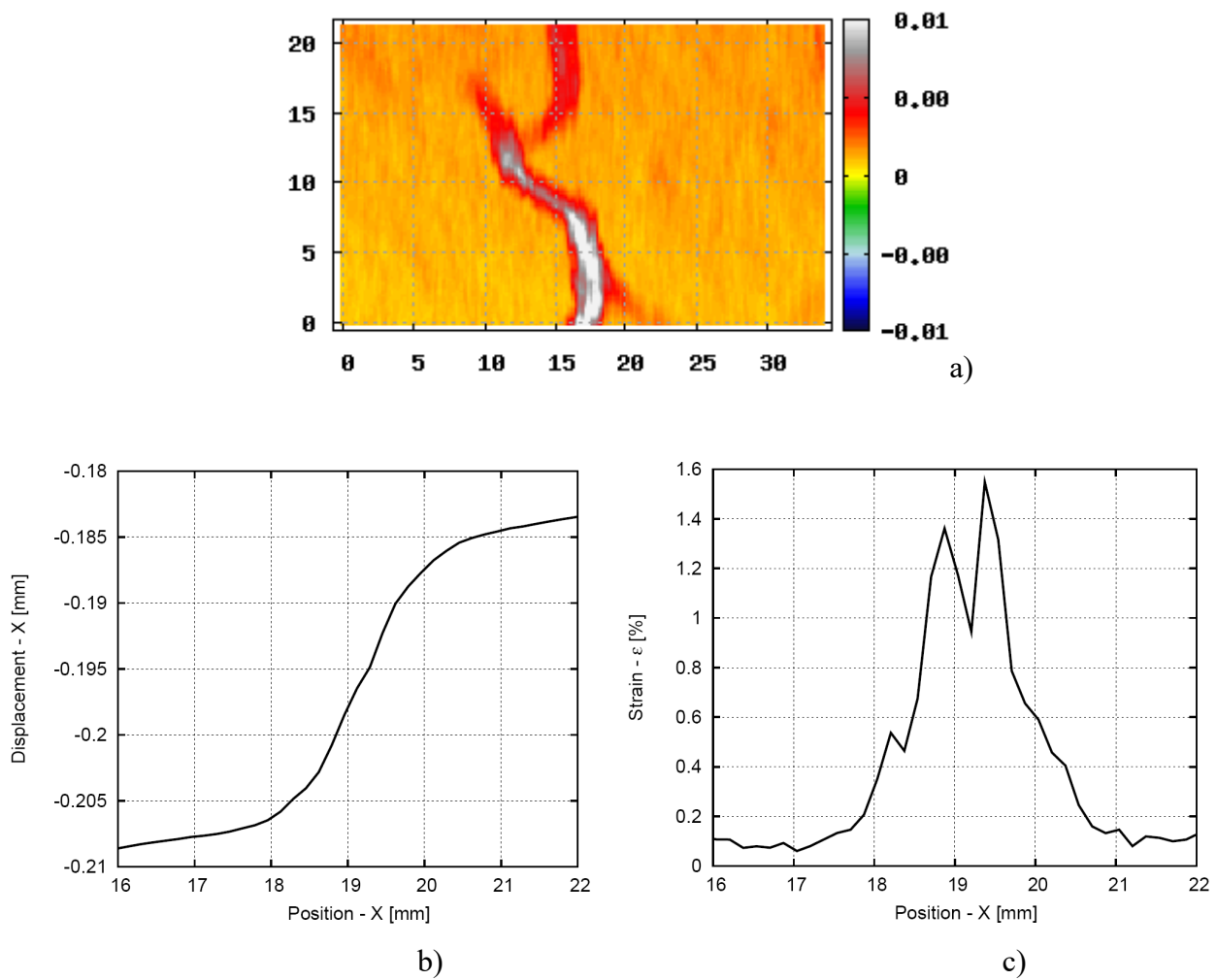
7

Fig.4: Measured localized zone above beam notch: a) image, b) horizontal displacement profile and c) horizontal normal strain profile across zone at peak load (image length resolution 90 pixel/mm, search patch size 180 pixels, distance between search patch centres 15 pixels) based on own software [9] (vertical and horizontal axes in 'a' denote coordinates in [mm] and colour scale strain intensity)
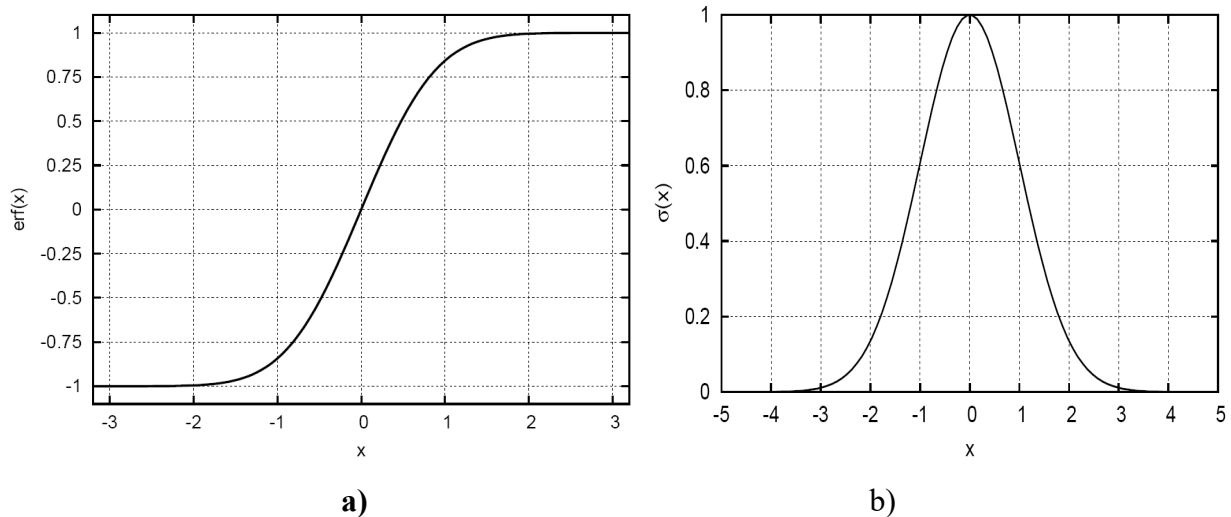
a)　　　　　　　　　　　　　　**b)**

Fig.5: Evolution of error function (a) and normal distribution (Gauss) function versus variable x

The measured displacements in Figs.6 and 7 are the same for various search patch sizes when using our software [8] and commercial software [22] (Fig.8Aa and 8Ab). In turn, the strains are similar when using the commercial software [22] (Fig.8Bb) and strongly affected by search patch size using our software [8] (Fig.8Ba). The fitting function parameter σ in Tab.1 always strongly depends on the search patch size independently of Eqs.1 and 2. In turn, the fitting function parameter σ in Tab.2 is almost the same if a normal distribution fitting function is used to describe the horizontal normal strain. The fitting function parameters σ are different with the both methods (Tabs.1 and 2). The parameters σ determined by the software VIC-2D [22] are different with Eqs.1 and 2 (the discrepancies are almost 300%). In turn, these discrepancies are negligible (only 15%), when the own software was used [8], [9].

Effect of distance between search patch centres

The effect of the distance between search patch centres on the width of localized zones based on the horizontal displacement and horizontal normal strain above the beam notch is shown in Figs.9 and 10, using the high length resolution of 90 pixels/mm and search patch size of 120 pixels. This effect is also shown at two different length resolutions in Tabs.3 and 4, when the measured surface displacements were again fitted by the error function (Eq.1) and the surface strains fitted by the normal distribution (Gauss) function (Eq.2).
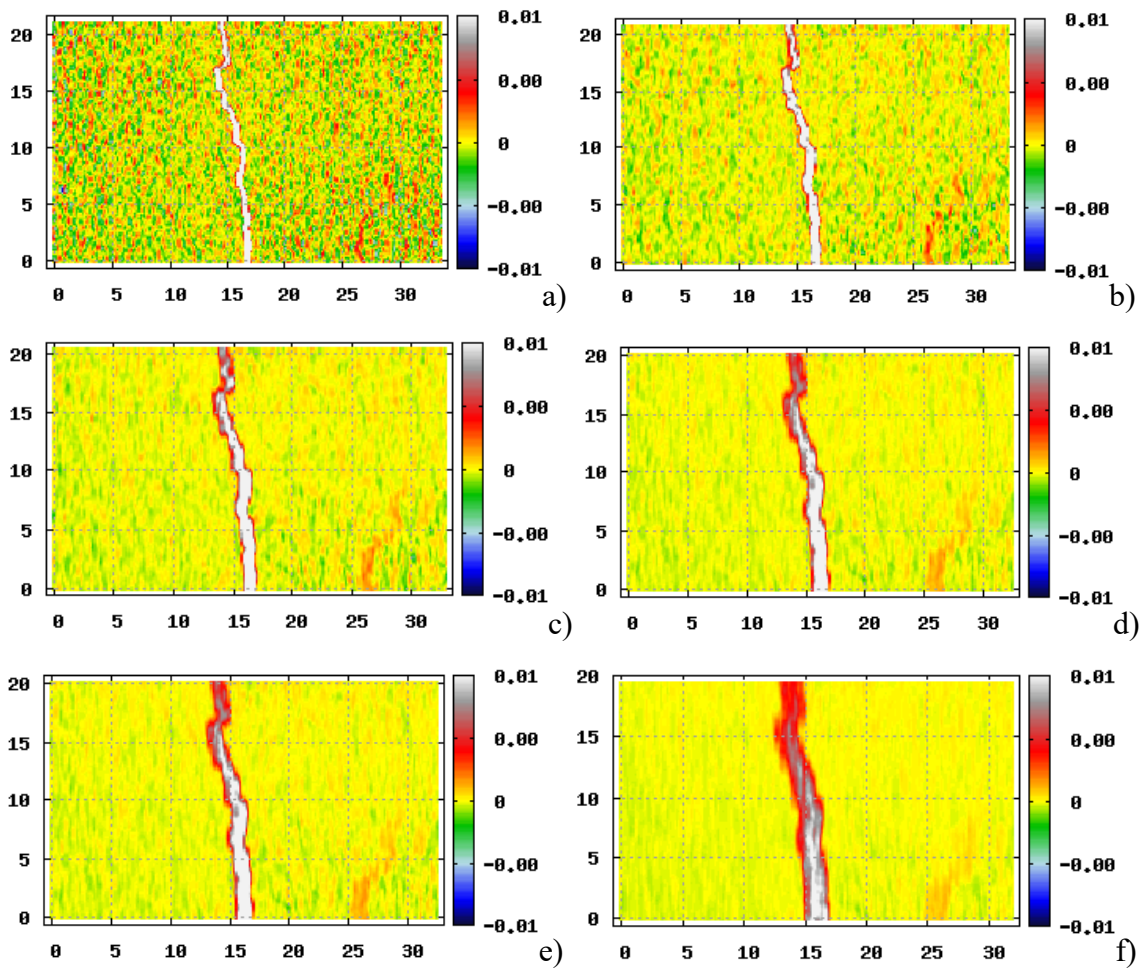
9

Fig.6: Localized zones directly above notch at peak load in experiments with fine-grained concrete notched beam 'A1' based on horizontal normal strain obtained by means of own software [9] with high length resolution of 90 pixels/mm and search patch distance of 15 pixels at various search patch size: a) 30 pixels, b) 60 pixels, c) 90 pixels, d) 120 pixels, e) 150 pixels and f) 180 pixels (vertical and horizontal axes denote coordinates in [mm] and colour scale strain intensity)

The measured displacements are similar with the various search patch distance when using both programmes [8], [9] and [22] (Fig.11A). However, the horizontal normal strain is not affected by the search patch distance with the own software [8], [9] only (Fig.11Ba), whereas is affected when the commercial software [22] was applied (Fig.11Bb). It means that in calculations with our software [8], [9], the function parameter σ does not depend on the search patch distance in the case of the error or normal distribution fitting function (Tab.3). In turn, in calculations with the commercial software [22], the fitting function parameter σ depends on the search patch distance when a normal distribution function is used to describe the horizontal normal strain distribution (Tab.4). The fitting function parameters σ are again different with the both methods (Tabs.3 and 4).

10

The parameters σ determined by VIC-2D [22] are different with Eqs.1 and 2 (the discrepancies are almost 400%). In turn, these discrepancies are again negligible (only 15%), when the own software was used [8], [9].
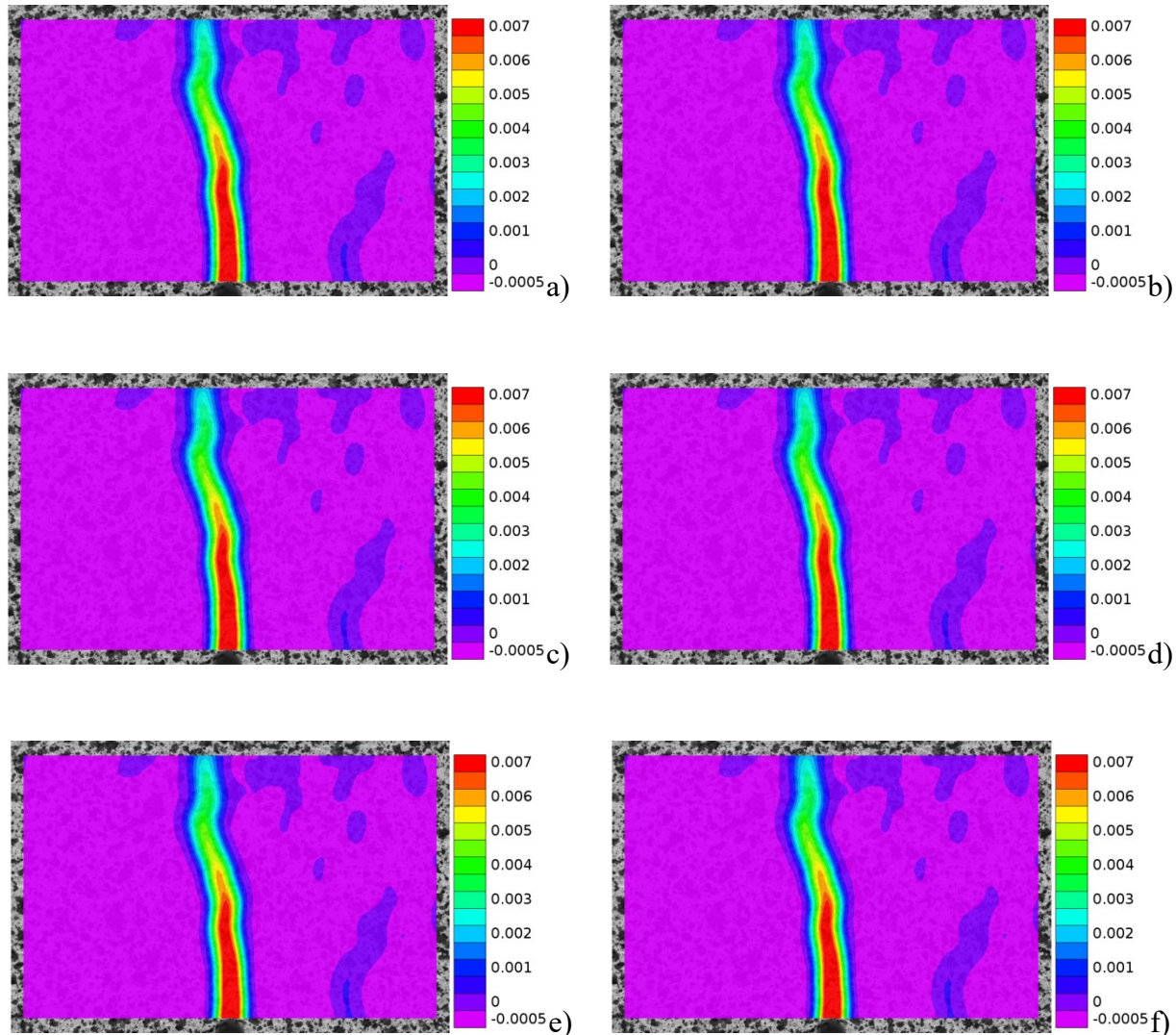

Fig.7: Localized zones directly above notch at peak load in experiments with fine-grained concrete notched beam 'A1' based on horizontal normal strain obtained by means of commercial software VIC-2D [22] with high length resolution of 90 pixels/mm and search patch distance of 15 pixels at various search patch sizes: a) 30 pixels, b) 60 pixels, c) 90 pixels, d) 120 pixels, e) 150 pixels and f) 180 pixels (vertical axis denotes colour scale strain intensity)
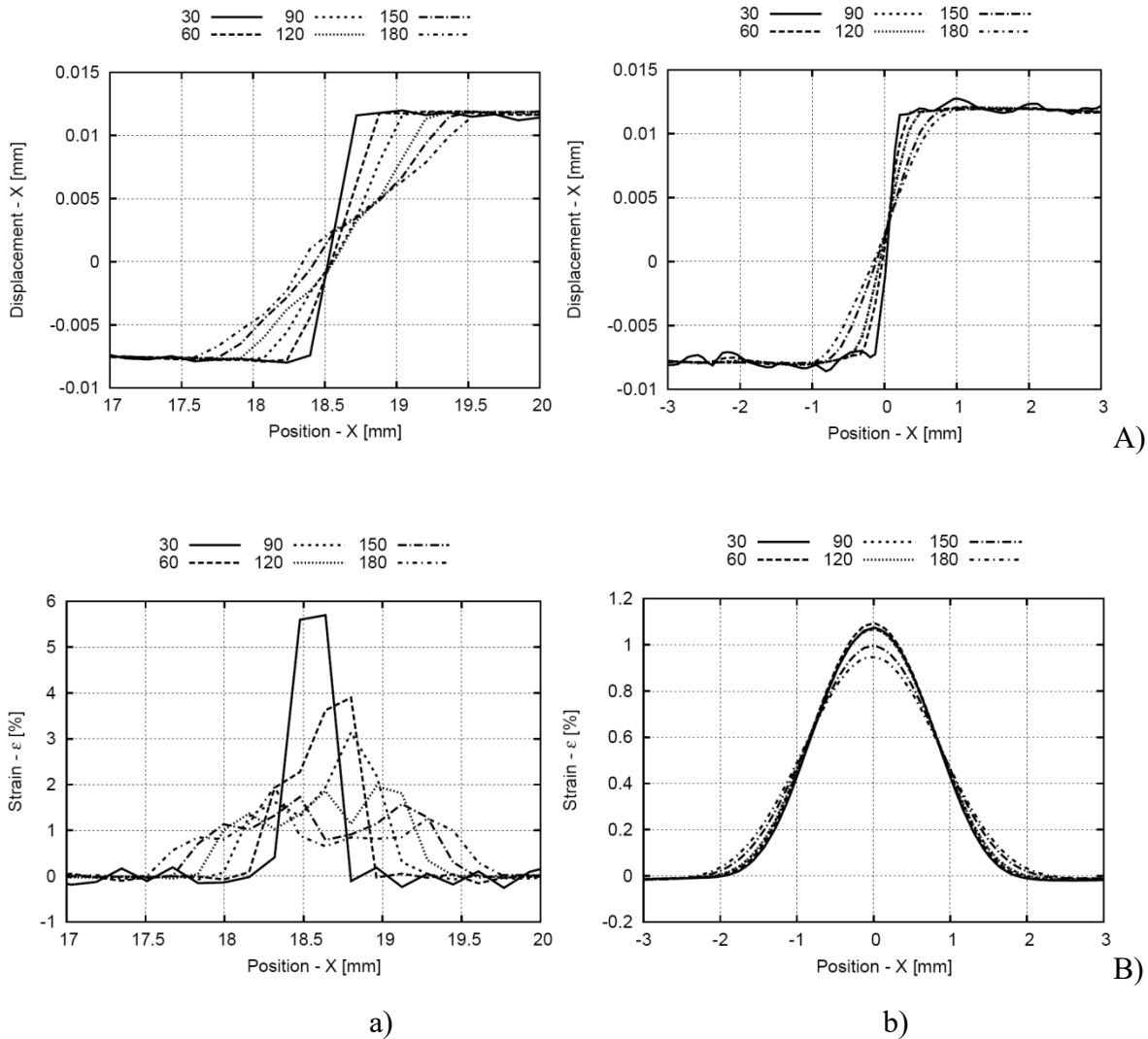
Fig.8: Horizontal displacement profiles (A) and calculated horizontal normal strain profiles (B) across localized zone above beam notch 'A1' at peak load with different search patch sizes in pixels (image length resolution 90 pixels/mm, and search patch distance15 pixels: a) generated by own software [8], [9]) and b) generated by commercial software [22]

Effect of length resolution

The effect of the image length resolution (30 pixel/mm and 90 pixel/mm) on the experimental results at peak load can be determined from Tabs.1-4. When using the own [8] and commercial software [22], the fitting function parameters σ (Eqs.1 and 2) are always greater at the lower (30 pixel/mm) than at the higher (90 pixel/mm) length resolution. If we increase three times the length resolution, we obtain the higher fitting function parameters σ by the factor 3.

Tab.1: Error and normal distribution (Gauss) function parameter σ (Eqs.1 and 2) using images from 5 beam experiments at different search patch size and length resolutions with search patch distance 15 pixels (using our software [8], [9])

Search patch size [pixel]	Search patch distance [pixel]	Beam 'A1' length resolution 90 pixel/mm		Beam 'A2' length resolution 90 pixel/mm		Beam 'A3' length resolution 90 pixel/mm		Beam 'B1' length resolution 30 pixel/mm		Beam 'B2' length resolution 30 pixel/mm	
		ERF [mm]	Gauss [mm]	ERF [mm]	Gauss [mm]	ERF [mm]	Gauss [mm]	ERF [mm]	Gauss [mm]	ERF [mm]	Gauss [mm]
30	15	0.067	0.084	0.425	0.334	0.481	0.421	0.276	0.265	0.289	0.273
60	15	0.185	0.197	0.447	0.389	0.532	0.475	0.619	0.562	0.556	0.554
90	15	0.298	0.311	0.496	0.421	0.634	0.586	0.947	0.866	0.892	0.876
120	15	0.424	0.455	0.560	0.473	0.743	0.692	1.313	1.265	1.222	1.263
150	15	0.552	0.577	0.635	0.570	0.812	0.775	1.733	1.755	1.601	1.658
180	15	0.669	0.679	0.743	0.710	0.857	0.811	2.128	2.258	1.959	2.005

Tab.2: Error and normal distribution (Gauss) function parameter σ (Eqs.1 and 2) using images from 5 beam experiments at different search patch size and length resolutions with search patch distance 15 pixels (using commercial software [22])

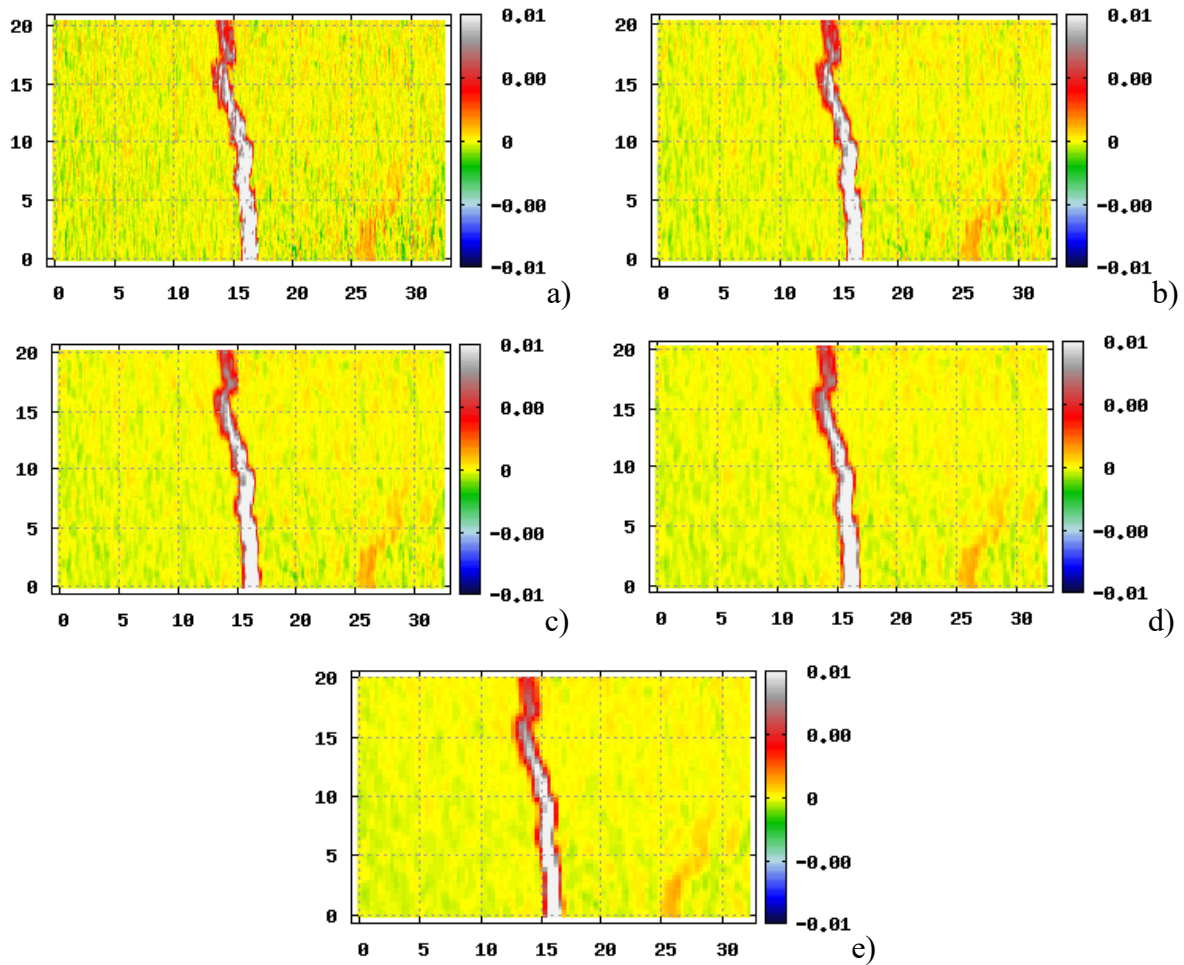| Search patch size [pixel]	Search patch distance [pixel]	Beam 'A1' length resolution 90 pixel/mm		Beam 'A2' length resolution 90 pixel/mm		Beam 'A3' length resolution 90 pixel/mm		Beam 'B1' length resolution 30 pixel/mm		Beam 'B2' length resolution 30 pixel/mm	
		ERF [mm]	Gauss [mm]	ERF [mm]	Gauss [mm]	ERF [mm]	Gauss [mm]	ERF [mm]	Gauss [mm]	ERF [mm]	Gauss [mm]
30	15	0.105	0.711	0.615	0.879	0.281	0.811	0.476	2.172	0.484	2.181
60	15	0.186	0.721	0.613	0.881	0.353	0.835	0.664	2.203	0.827	2.207
90	15	0.258	0.738	0.611	0.876	0.472	0.866	0.842	2.254	1.129	2.286
120	15	0.316	0.739	0.613	0.876	0.589	0.892	1.044	2.326	1.462	2.401
150	15	0.401	0.791	0.621	0.877	0.715	0.915	1.284	2.423	1.769	2.535
180	15	0.484	0.831	0.622	0.879	0.817	0.941	1.536	2.541	2.139	2.707

Fig.9: Localized zones directly above notch at peak load in experiments with fine-grained concrete notched beam 'A1' based on horizontal normal strain using own software [8], [9] with high length resolution of 90 pixels/mm and search patch size of 120 pixels at various search patch distance: a) 5 pixels, b) 10 pixels, c) 15 pixels, d) 20 pixels and e) 30 pixels (vertical and horizontal axes denote coordinates in [mm] and colour scale strain intensity)

At the length resolution of 90 pixel/mm and the search patch size of 90 pixels (beam 'A1'), the parameter σ was: 0.298 (Eq.1) and 0.311 (Eq.2) using the own software [8], and 0.258 (Eq.1) and 0.738 (Eq.2) using the commercial software [22] (Tabs.1 and 2). In turn, at the length resolution of 30 pixel/mm (beam 'B1'), the parameter σ was: 0.947 (Eq.1) and 0.866 (Eq.2) using the own software [9], and 0.842 (Eq.1) and 2.254 (Eq.2) using the commercial software [22] (Tabs.1 and 2).
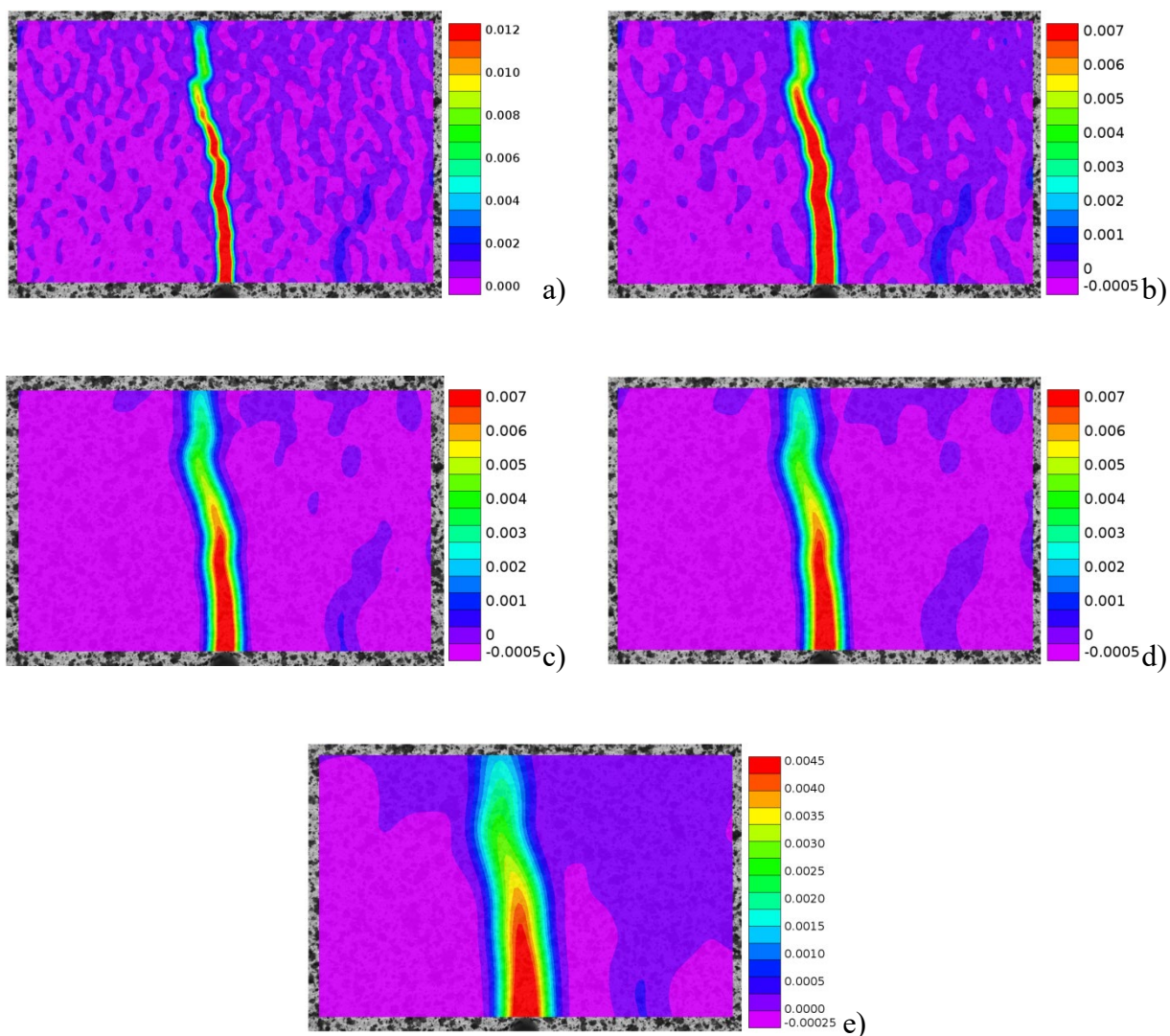
14

Fig.10: Localized zones directly above notch in experiments with fine-grained concrete notched beam 'A1' based on horizontal normal strain using commercial software [22] with high length resolution of 90 pixels/mm and search patch size of 120 pixels at various search patch distance: a) 5 pixels, b) 10 pixels, c) 15 pixels, d) 20 pixels and e) 30 pixels (vertical axis denotes colour scale strain intensity)
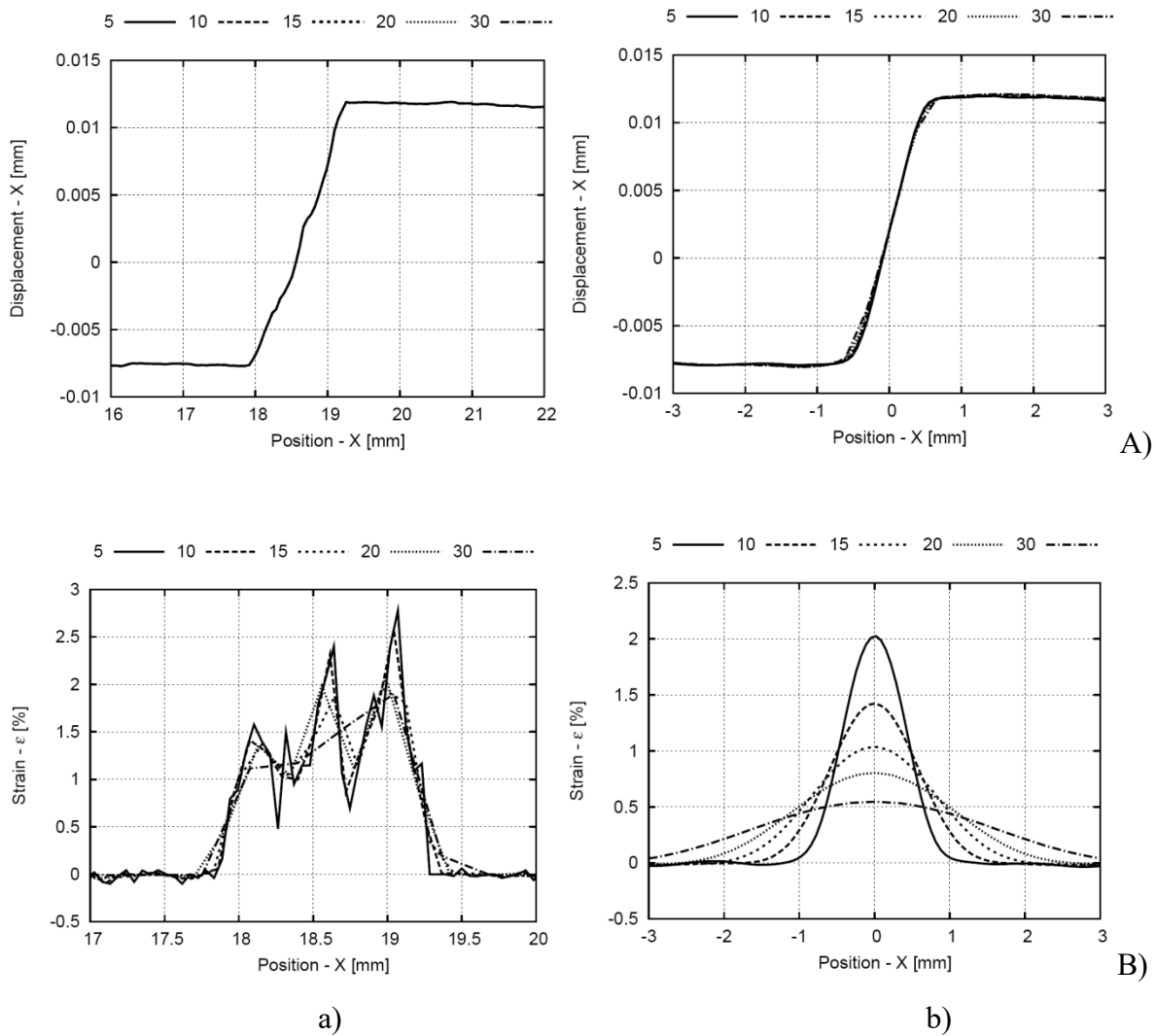
Fig.11: Horizontal displacement profiles (A) and calculated horizontal normal strain profiles (B) across localized zone above beam notch 'A1' at peak load with different search patch distance in pixels (image length resolution 90 pixels/mm, search patch size 120 pixels): a) own software [8], [9] and b) commercial software [22]

Tab.3: Error and normal distribution (Gauss) function parameter σ (Eqs.1 and 2) using images from beam experiments at different search patch distance between and length resolutions with search patch size 120 pixels (using own software [8], [9])

Search patch size [pixel]	Search patch distance [pixel]	Beam 'A1' length resolution 90 pixel/mm		Beam 'A2' length resolution 90 pixel/mm		Beam 'A3' length resolution 90 pixel/mm		Beam 'B1' length resolution 30 pixel/mm		Beam 'B2' length resolution 30 pixel/mm	
		ERF [mm]	Gauss [mm]	ERF [mm]	Gauss [mm]	ERF [mm]	Gauss [mm]	ERF [mm]	Gauss [mm]	ERF [mm]	Gauss [mm]
120	5	0.406	0.455	0.559	0.479	0.713	0.691	1.225	1.279	1.301	1.266
120	10	0.408	0.455	0.553	0.478	0.727	0.718	1.229	1.283	1.306	1.261
120	15	0.424	0.455	0.560	0.473	0.743	0.692	1.222	1.263	1.313	1.265
120	20	0.397	0.449	0.571	0.474	0.752	0.728	1.216	1.298	1.342	1.293
120	30	0.407	0.449	0.568	0.489	0.787	0.752	1.254	1.285	1.351	1.300

Tab.4: Error and normal distribution (Gauss) function parameter σ (Eqs.1 and 2) using images from beam experiments at different search patch distance between and length resolutions with search patch size 120 pixels (using commercial software [22])

Search patch size [pixel]	Search patch distance [pixel]	Beam 'A1' length resolution 90 pixel/mm		Beam 'A2' length resolution 90 pixel/mm		Beam 'A3' length resolution 90 pixel/mm		Beam 'B1' length resolution 30 pixel/mm		Beam 'B2' length resolution 30 pixel/mm	
		ERF [mm]	Gauss [mm]	ERF [mm]	Gauss [mm]	ERF [mm]	Gauss [mm]	ERF [mm]	Gauss [mm]	ERF [mm]	Gauss [mm]
120	5	0.312	0.389	0.660	0.516	0.441	0.611	1.019	1.186	1.442	1.243
120	10	0.323	0.559	0.679	0.687	0.515	0.748	1.036	1.687	1.449	1.758
120	15	0.316	0.739	0.613	0.876	0.589	0.892	1.044	2.326	1.462	2.401
120	20	0.342	0.973	0.685	1.121	0.673	1.211	1.057	3.013	1.461	3.063
120	30	0.353	1.406	0.769	1.649	0.733	1.847	1.181	4.459	1.531	4.598

17

4.2 Discussion

The experimental results of Section 4.1 clearly show that the width of a localized zone wc in concrete cannot be determined based on colour post-processing DIC images (Fig.4). The fitting function parameters σ (Eqs.1 and 2) become e.g. always greater with decreasing length resolutions independently of the software used. Thus, the width of a localized zone is larger. At the same length resolution, the results obtained within the own software [8], [9] do not depend on the search patch distance and depend on the search patch size for displacements and strains (Tabs.1 and 3). In turn, the results obtained with the commercial software VIC-2D [22] do not depend on the search patch size for displacements and depend on the search patch distance for strains (Tabs.2 and 4). In addition, it is difficult to determine precisely the edges of a localize zone based on actual experimental images (Fig.4). In order to avoid the effect of both the search patch size (Section 4.1) and the cut-off value at displacement and strain profiles (Fig.4), a method was proposed to determine uniformly the width of a localized zone in concrete (described below in Section 5).

5. Determination of width of localized zone

In order to determine the width of a localized zone, we used the results of the own software [8], [9] since the fitting parameters σ were similar independently of the assumed fitting function. For the evaluation, we chose the images of beams at the peak load with the highest length resolution (90 pixel/mm). The smallest possible patch size was assumed to be bigger at least by 1 pixel than the biggest speckle used [36], [37], i.e. $\geq$90 pixels. The measured surface displacements were always fitted in parallel by the error function (Eq.1) and the surface strains by the normal distribution (Gauss) function (Eq.2). The fitting function parameter σ in Eqs.1 and 2 was calculated as the average value, σ_{avr}, of results for the search patch sizes: 90, 120, 150 and 180 pixels (the results are similar with Eqs.1 and 2). For calculation purposes, artificially generated localized zones in experimental images were created with the known width wc. Several artificial localized zones with the width wca of 1 mm, 2 mm, 4 mm and 6 mm were manually generated from laboratory experiment images (with the high length resolution of 90 pixel/mm). The images were edited using the GIMP program (GNU Image Manipulation Program), being a freely distributed program used for photo retouching, image composition and image authoring. The image mid-sections were stretched to obtain the assumed width of a localized zone. The strain distribution was described by a Gauss-shaped function (Eq.2) as in experimental images. Next, the average fitting parameter for

18

artificial images, σ^a_{avr}, was calculated. A generation of artificial images allowed us for determining the multiplier m to obtain the assumed width of a localized zone w_c^a in artificial images

$$m = w_c^a / \sigma^a_{avr} = 4.0$$

(3)

Thus, the width of a localized zone in beam experiments could be determined as wc=4.0×σ_{avr}. In this case, 95% of values of the normal distribution function area were within the distance of two standard deviations in both directions from the mean value (Fig.12). The same multiplier m of Eq.3 can be also used in the displacement analyses.
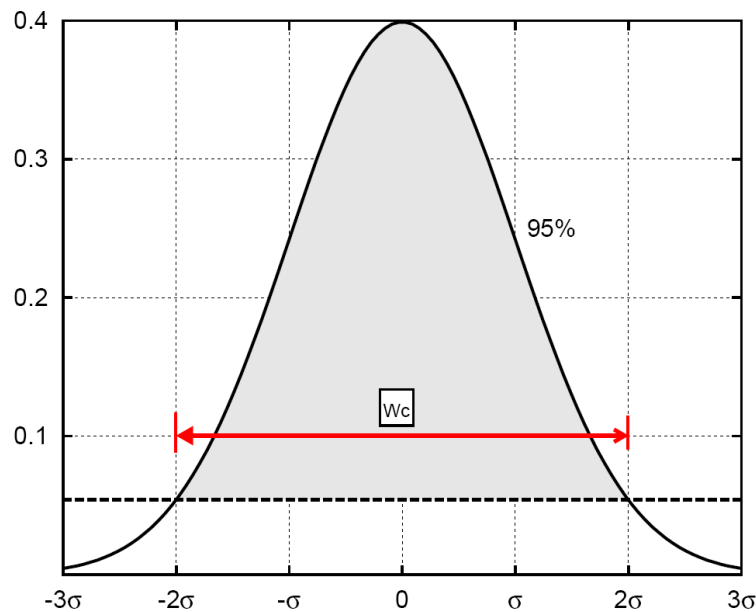
Fig.12: Determination of width of localized zone wc based on normal distribution function (Eq.2) describing experimental horizontal normal strain distribution

With the multiplier m=4.0 determined with the help of artificial localized zones (Eq.3) and the results of σ_{avr} from Tab.1 for experimental images at the length resolution of 90 pixel/mm and search patch size higher than 90 pixels, the maximum width of a localized zone in concrete beams at the peak load was (w_c=4.0×σ_{avr}): w_c=2.0 mm in the beam 'A1' (1×d_{max} and 4×d_{50}), w_c=2.4 mm in the beam 'A2' (1.2×d_{max} and 5×d_{50}) and w_c=2.4 mm in the beam 'A2' (1.2×d_{max} and 5×d_{50}) and w_c=3 mm in the beam 'A3' (1.5×d_{max} and 6×d_{50}). These width values in [mm] are similar as the measured in [32] using DIC (2.8 mm = 0.35×d_{max}), but are smaller than the obtained in experiments using the acoustic emission (40-70 mm) [6], [33], [35], X-rays (45 mm = 4×d_{max}) [35] or SEM (33

19

mm = 2.35×d_{max}) [15]. Note that for higher image length resolutions, the multiplier '4' in Eq.3 may slightly change.

Summarized, the DIC technique proposed for concrete should be performed as follows:

- polish surface of the concrete specimen to achieve a smooth surface and then cover the specimen surface with the white paint,
- make an irregular speckle pattern on the surface of the analyzed concrete specimen using the black spray with the smallest possible speckles (other techniques as e.g. printer ink can be also used [11], [14]),
- put the camera in the front of the concrete specimen on a tripod to ensure a stable position. The camera should be perpendicular to the analyzed specimen.
- place the camera lenses as close to the investigated surface as possible to obtain a high pixel/mm ratio (e.g. 90 pixels/mm),
- take a reference image of a visible concrete surface in order to determine the length resolution in pixels per mm,
- make frequently images during a deformation process,
- chose a search patch size bigger at least by 1 pixel than the biggest speckle available in the speckle pattern,
- plot displacement and strain profiles for different search patch sizes,
- fit the error and normal distribution function (Eqs.1 and 2) to determine the displacement and strain profiles (calculate σ and σ_{avr}),
- calculate the fitting parameter σ for artificially stretched experimental reference images with the prescribed width of a localized zone w_c^a,
- calculate the multiplier m (Eq.3) for artificially stretched experimental reference images,
- determine the width of a localized zone w_c in concrete specimens using the multiplier m from artificially stretched images and the average fitting function parameter σ^a_{avr} from experimental images.

In experiments, a localized zone was always created before the peak on the vertical force - horizontal CMOD diagram (Fig.13). It developed during a deformation process in the range of CMOD=0.02-0.07 mm until a discrete macro-crack was created at deflection of u/D=0.004 (Fig.13). The width of a localized zone first increased due to concrete dilatancy up to value w_c=2.0-3.0 mm at CMOD=0.015 mm and then slightly decreased in the range of CMOD=0.015-0.07 mm. Its

formation rate was strongly non-linear caused by a heterogeneous concrete structure. The length and height of a localized zone above the notch (measured for images with low length scale resolution) were l_c=65 mm and h_c=46 mm (h_c/D=0.575) at CMOD≈0.07 mm, respectively (Fig.14). To determine the appearance of a macro-crack, the additional beam tests were carried out with the prescribed vertical displacement at the mid-span. A horizontal displacement jump measured by means of the CMOD gauge was assumed to be equivalent with the occurrence of a macro-crack. A macro-cracks occurred when the horizontal CMOD displacement between the edges of a localized zone was about 0.06 mm.
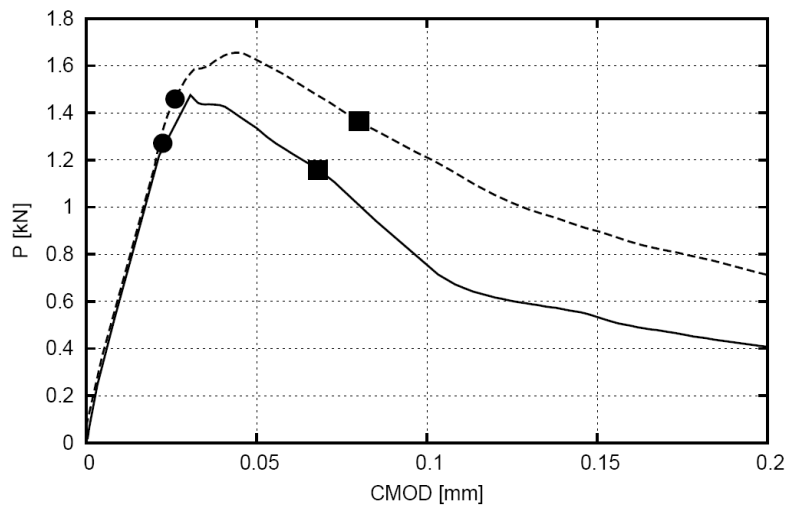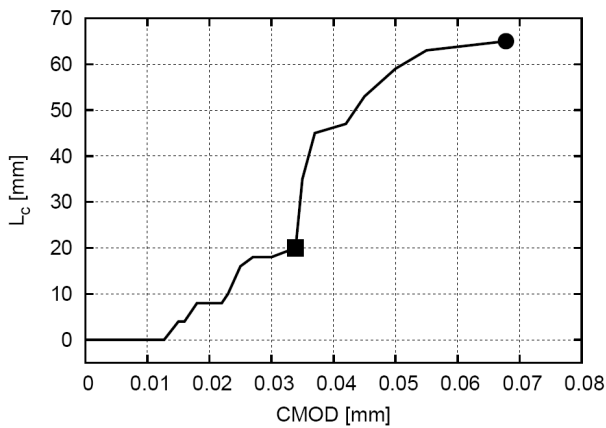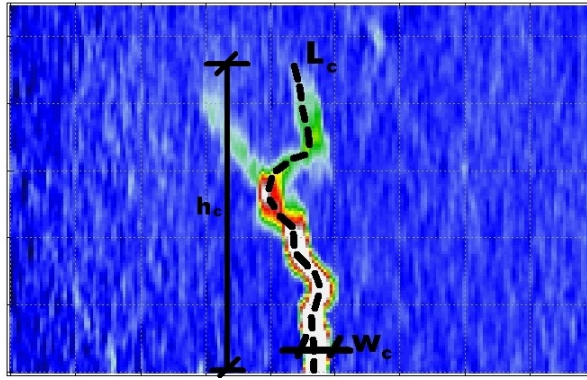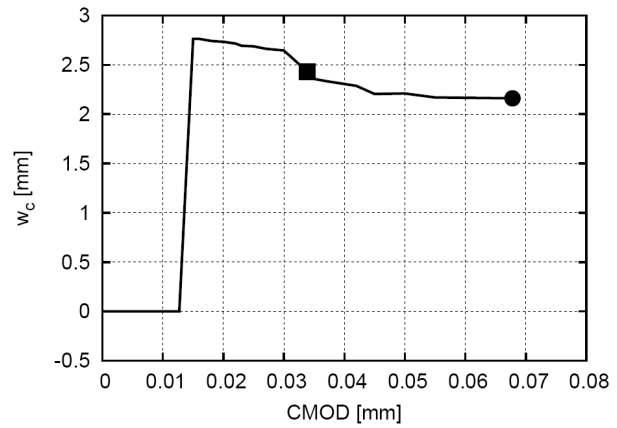

Fig.13: Formation of localized zone and macro-crack on vertical force P – horizontal CMOD diagram (● - appearance of localized zone, ■ - appearance of macro-crack)

Fig.14: Evolution of length L_c (a) and width w_c (b) of localized zone against CMOD in experiment with notched beam of fine-grained concrete based on DIC at image length resolution of 90 pixel/mm (■ - maximum vertical force P_{max}, ● - formation of macro-crack)

6. Conclusions

The following conclusions can be drawn from experiments with notched beams made from fine-grained concrete under quasi-static three-point bending using the Digital Image Correlation technique:

● The measured surface displacements due their small magnitude were very sensitive to the length resolution and search patch size of images. In particular, the effect of the length resolution is important and cannot be completely avoided. The higher image length resolution is obviously more advantageous. A method was proposed to determine precisely and uniformly the width of a localized zone.

• The width and length of a localized zone on the concrete surface of notched beams non-uniformly changed during a deformation process before a macro-crack formed due to a heterogeneous concrete composition. The maximum width of a localized zone at the peak load was approximately 2-3 mm [$(1.0-1.5) \times d_{max}$)]. The maximum ratio between the height of a localized zone and effective beam height was about 0.6. A macro-crack occurred in a softening regime for CMOD displacements about two times larger than at the peak load.

• Due to discrepancies in the measured width of localized zones in concrete using different measurement techniques (DIC, acoustic emission, X-rays, SEM), this problem merits further experimental investigations.

References

[1] Bažant Z. and Planas J (1998) Fracture and size effect in concrete and other quasi-brittle materials. CRC Press LLC, Boca Raton.

[2] Lilliu G and van Mier JGM (2003) 3D lattice type fracture model for concrete. Engineering Fracture Mechanics, 70:927-941.

[3] Tejchman J. and Bobiński J. (2013) Continuous and discontinuous modeling of fracture in concrete using FEM. Springer, Berlin-Heidelberg (eds. W. Wu and R. I. Borja), http://dx.doi.org/10.1007/978-3-642-28463-2.

[4] Bažant, ZP and Oh, BH Crack band theory for fracture of concrete. Material Structures, RILEM 16:155.177, 1983.

[5] Pijauder-Cabot, G. and Bažant, ZP Non-local damage theory. ASCE Journal of Engineering Mechanics, 113:1512-1533, 1987.

[6] Zhang D and Wu K (1999) Fracture process zone of notched three-point-bending beams. Cement and Concrete Research, 29:1887-1892.

[7] Bhandari AR and Inoue J (2005) Experimental study of strain rates effects on strain localization characteristics of soft rocks. Soils and Foundations, 45:125-140.

[8] Kozicki J and Tejchman J (2007) Experimental investigations of strain localization in concrete using Digital Image Correlation (DIC) technique. Archives of Hydro-Engineering and Environmental Mechanics, 54:3-24.

[9] Skarżyński Ł, Syroka E and Tejchman J (2011) Measurements and calculations of the width of fracture process zones on the surface of notched concrete beams. Strain, 47:319-332.

[10] Shah SG and Chandra Kishen JM (2010) Fracture Properties of Concrete-Concrete Interfaces Using Digital Image Correlation. Experimental Mechanics, doi 10.1007/s11340-010-9358-y.

[11] Alam SY, Loukili A and Grondin F (2012) Monitoring size effect on crack opening in concrete by Digital Image Correlation. European Journal of Environmental and Civil Engineering (in press).

[12] Hu XZ and Wittmann FH (1990) Experimental method to determine extension of fracture process zone. Journal of Materials in Civil Engineering, 2:15-23.

[13] Nemati KM (1997) Fracture analysis of concrete using scanning electron microscopy, Scanning, 19:426-430.

[14] Diamond S and Mindess SA (1980) Preliminary SEM study of crack propagation in mortar. Cement Concrete Research, 10:509-519.

[15] Hadjab H, Chabaat SM and Thimus JF (2007) Use of Scanning Electron Microscope and the Non-local Damage Model to Investigate Fracture Process Zone in Notched Concrete Beams, Experimental Mechanics, 47:473-484.

[16] Maji A, Ouyang C and Shah SP (1990) Fracture mechanisms of concrete based on acoustic emission. Journal of Materials Research, 5:206-217.

[17] Carpinteri A and Lacidogna G (2003) Damage diagnostic in concrete and masonry structures by acoustic emission technique. Automatic Control and Robotics, 3:755-764.

[18] Haidar K, Pijauder-Cabot G, Dube JF and Loukili A (2005) Correlation between the internal length, the fracture process zone and size effect in model materials. Materials and Structures, 38:201-210.

[19] Vavrik D, Fila T, Jandejsek I and Vasely V (2012) X-ray observation of the loaded silicate composite. 18th International Conference Engineering Mechanics 2012, Svratka, Czech Republic, May 14-17.

[20] Bornert M, Brémand F, Doumalin P, Dupré JC, Fazzini M, Grédiac M, Hild F, Mistou S, Molimard J, Orteu JJ, Robert L, Surrel Y, Vacher P and Wattrisse B (2009) Assessment of digital image correlation measurement errors: methodology and results. Experimental Mechanics, 49:353–370.

[21] Helm JD, McNeill SR and Sutton MA (1996) Improved 3D image correlation for surface displacement measurement. Optical Engineering, 35:1911–1920.

[22] Vic-2D-2009-Guide. Correlated Solutions, 2009.

[23] Skarżyński Ł and Tejchman J (2010) Calculations of fracture process zones on meso-scale in notched concrete beams subjected to three-point bending. European Journal of Mechanics A/Solids, 29:746-760.

[24] Medina A., Cordova JA, Luna E and Trevino E (1998) Velocity field measurements in granular gravity flow in a near 2D silo. Applied Physics Letters, 250:111-116.

[25] White DJ., Take WA and Bolton MD (2003) Soil deformation measurement using particle image velocimetry (PIV) and photogrammetry. Geotechnique, 53:619-631.

[26] Rechenmacher AL and Finno RJ (2004) Digital image correlation to evaluate shear banding in dilative sands. Geotechnical Testing Journal 27:13-22.

[27] Chehab GR, Seo Y, Kim YR (2007) Viscoelastoplastic damage characterization of asphalt-aggregate mixtures using digital image correlation. International Journal of Geomechanics ASCE 7:111–118.

[28] Robert L, Nazaret F, Cutard T and Orteu JJ (2007) Use of 3-D Digital Image Correlation to characterize the mechanical behavior of a fiber reinforced refactory castable. Experimental Mechanics, 47:761-773.

[29] Ferreira MDC, Venturini WS and Hild F (2011) On the analysis of notched concrete beams: From measurement with Digital Image Correlation to identification Boundary Element Method of a cohesive model. Engineering Fracture Mechanics, 78:71-84.

[30] Choi S and Shah SP (1997) Measurements of Deformations on Concrete Subjected to Compression Using Image Correlation. Experimental Mechanics, 37:307-313.

[31] Corr G, Accardi M, Graham-Brady L and Shah S (2007) Digital image correlation analysis of interfacial debonding properties and fracture behavior in concrete. Engineering Fracture Mechanics, 74:109-121.

[32] Wu Z, Rong H, Zheng J and Dong W (2011) An experimental investigation on the FPZ properties in concrete using digital image correlation technique. Engineering Fracture Mechanics, 78:2978-2990.

[33] Mihashi H and Nomura N (1996) Correlation between characteristics of fracture process zone and tension-softening properties of conctere. Nuclear Engineering and Design, 165:359-376.

[34] Hadjab, H. Fracture process zone in concrete beams: experimental investigation and numerical modelling. Proc. of the SEM Annual Conference, June 1-4, Albuquerque New Mexico USA, 2009.

[35] Otsuka K and Date H (2000) Fracture process zone in concrete tension specimen. Engineering Fracture Mechanics, 65:111-131.

[36] Lecompte D, Smits A, Bossuyt S, Sol H, Vantomme J, van Hemelrijck D, Habraken AM (2006) Quality assessment of speckle patterns for digital image correlation. Optical and Lasers in Engineering, 44:1132-1145.

[37] Pan B, Xie H, Wang Z, Qian K and Wang Z (2008) Study on subset size selection in digital image correlation for speckle patterns. Optics Express, 16:7037-7048.